Proceedings of the 2014 IEEE
International Conference on Robotics and Biomimetics
December 5-10, 2014, Bali, Indonesia

# Aerial Posture Adjustment of a Bio-Inspired Jumping Robot for Safe Landing: Modeling and Simulation

Jun Zhang, Xi Yang, Ying Zhang, Guifang Qiao, Guangming Song, and Aiguo Song

*Abstract*—**The aerial posture adjustment of jumping robots are very important for them to land safely. The body of our previous jumping robot rotates in the air which may lead to damage of its fragile parts during landing. In this paper, the aerial posture adjustment of the robot is investigated by modeling and simulation. Firstly, inspired by aerial posture adjustment of animals and insects, the robot model with a pole leg and an additional weight (AW) is introduced. Then, the simulations of the model are conducted. Specifically, the jumping without and with active posture adjusting in the air are simulated. The effects of the length of the pole leg, the mass of the AW, and the leg's driving torque on aerial posture adjusting performances are studied. The simulation results show that the active adjusting with the pole leg system can change the aerial posture of the robot and make it land with a safe posture with proper adjusting the parameters. The results of this paper verify the feasibility of the proposed aerial posture adjustment method which will help us to develop more robust jumping robot for applications in unstructured environments.**

## I. Introduction

JUMPING locomotion of animals, such as kangaroos, froghoppers, locusts, and fleas can help them to move from one location to another efficiently. This explosive movement also enable them escape from their natural enemies quickly. Inspired by jumping creatures, researchers have developed many bio-inspired jumping robots [1-4] which can leap over obstacles several times taller than themselves and have potential applications, for instance, planetary exploration [5] and reconnaissance [6].

With the developments of relevant technologies, some key problems in jumping robot design including self-righting [7-9], steering [8-10], and takeoff angle adjusting [6, 11, 12] have been solved in some jumping robots enabling them to jump continuously to overcome obstacles. Although many kinds of jumping robots have been developed, the widespread use of these robots still has some key technologies needing to be investigated. One of them is safe landing.

There are two mainly adopted strategies for jumping robots to avoid damage during landing. One is the devices with light weight and elastic properties are mounted around the robots to protect them from damage. This strategy can be seen as a passive method. For example, the Jollbot [13], the EPFL robot [8], and the jumping and rolling robot [14] have elastic cages around their bodies. The wheeled and jumping hybrid robots [15, 16] can use wheels to protect their jumping mechanisms.

Even though jumping robots with small sizes and light masses, or low jumping height using this strategy can operate well in many conditions. However, their jumping height drops dramatically when they are added with many electrical devices such as the battery, the control board, sensors, and cameras for practical applications. The safe landing problem is becoming obviously with heavier masses. Also, the passive method cannot control the posture of the robot which means that the robot will roll wildly after landing. Hence, the passive method cannot meet the requirements when a jumping robot with big size and heavy weight need a high jumping height and safe landing capability.

The other kind of strategy is the active posture adjustment in the air which can let the robot land with a safe posture. The hard parts of the robot contacts with the ground during landing will protect the fragile parts of the robot from damage. This method is inspired by the animals and insects in nature such as lemurs [17], cats [18], geckos [19], lizards [20], wingless pea aphids [21] and locust [22]. Animals rotate their legs and tails to active adjust their body posture in the air.

Inspired by animals, researchers have developed some robots which have similar aerial posture adjustment ability like animals. The four wheeled robot Tailbot [23] uses a tail like lizards to control its body posture before landing. A. M. Johnson et al developed a tail mechanism for the four legged robot X-RHex Lite [24]. This mechanism helps the robot to maneuver its body orientation for self-righting in the air and safe landing after running off a cliff. The new MSU jumping robot in [25] can control its body angle using its tail for aerial maneuvering. The tails of these robots can only rotate in a limited angle range relative to their bodies.

Our previous jumping robot [26] with weight of 132 g can jump about 100 cm high. Its landing postures are different with different structure parameters, mass distributions, and ground friction forces. Lower leg of the robot may damage when it contacts with the rigid ground during landing of the robot. In this paper, the feasibility of aerial posture active adjustment for safe landing of the robot is investigated by modeling and simulation.

This work was supported in part by the Natural Science Foundation of China under Grant 61403079 and Grant 61375076, Natural Science Foundation of Jiangsu Province under Grant BK20140637, Fundamental Research Funds for the Central Universities under Grant 2242014R20018, and Jiangsu Planned Projects for Postdoctoral Research Funds under Grant 1302064B.

Jun Zhang, Xi Yang, Ying Zhang, Guifang Qiao, Guangming Song, and Aiguo Song are with the School of Instrument Science and Engineering, Southeast University, Nanjing 210096, China (e-mail: j-zhang@seu.edu.cn, yangxigreat@163.com, zhangying295@126.com, qiaoguifang@126.com, mikesong@seu.edu.cn, a.g.song@seu.edu.cn).

978-1-4799-7397-2/14/$31.00 © 2014 IEEE

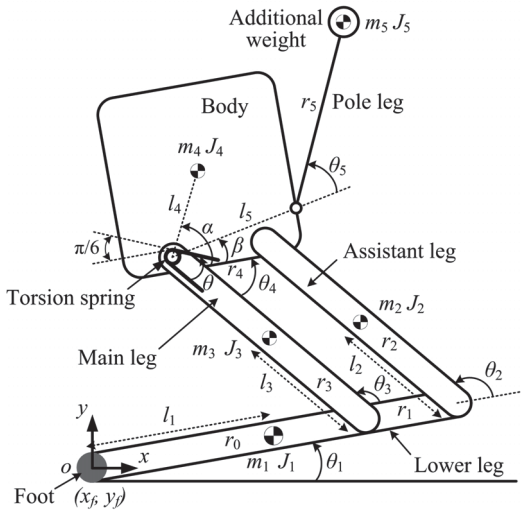


Fig. 1. New model of the jumping robot with a pole leg for aerial posture active adjusting.

## II. Mechanism and Posture Adjusting Method

### A. Jumping Mechanism

The jumping mechanism of the robot is a four-bar mechanism which consists of a body, a main leg, a lower leg, and an assistant leg as shown in Fig. 1. A torsion spring is mounted on the joint between the body and the main leg. The main leg swings around the joint to drive the four-bar mechanism. As the main leg rotating anticlockwise, the torsion spring is being loaded. After energy storing, an energy escapement mechanism is employed to trigger the four-bar mechanism to release the energy for jumping. A pole leg mechanism is mounted on the front surface of the body with an additional weight (AW) at its end point. The pole leg rotates around the joint between it and the body to adjust the posture of the robot in the air.

### B. Landing Posture Analysis

The robot rotates in the air and lands with different postures when the structural parameters of the four-bar mechanism are changed. Different landing postures have different influences on the jumping robot. The body of the robot has more stable structure than the lower leg. If the lower leg crashes onto the ground, the impact force is very large on the end point of the lower leg, this may lead to the damage of the lower leg. If the body touches the ground during landing, the fragile parts of the robot will be protected from damage. Hence, the aim of landing posture adjusting is to make the front surface of the robot touch the ground during landing.

### C. Aerial Posture Adjusting Method

The aerial posture active adjusting task is to identify the posture of the robot and control it to the condition that the hard parts contact the ground during landing. Before aerial posture adjusting, the robot needs to know its initial posture $p_0$, body rotation velocity $\omega$, and aerial flying time $T$. $p_0$ and $\omega$ can be detected through tilt sensor and gyroscope. The time $T$ is expressed as follows

$$T = 2v_0 \sin\theta_0 / g \tag{1}$$

where $v_0$ is the takeoff translational velocity and $\theta_0$ is the takeoff angle. In the air, the pole leg is controlled to rotate relate to the body. The robot is adjusted to the ideal posture.

After leaping into the air, the robot has the initial rotational velocity around its center of mass (COM). The posture adjusting problem is how to control the rotational speed of the pole leg's adjusting motor to change the rotational speed of the robot. In this paper, we mainly focus on the modeling and simulation of this problem.

## III. Modeling

### A. Kinematic Modeling

As shown in Fig. 1, the length of the lower leg is $(r_0 + r_1)$, the lengths of the assistant leg, the main leg, the body, and the pole leg are $r_2$ to $r_5$. $m_1$ to $m_5$ are the masses of the lower leg, the assistant leg, the main leg, the body, and the AW. The distances between the COMs of the masses and the joints are $l_1$ to $l_4$. $\theta_1$ to $\theta_5$ are variables for describing the positions and orientations of the bars and the pole leg. It is assumed that the contact point between the lower leg and the ground is an ideal hinge and there is no slippage between the lower leg and the ground. The positions of the COMs of the bars are as follows

$$\begin{cases} x_{c1} = x_f + l_1\cos\theta_1 \\ y_{c1} = y_f + l_1\sin\theta_1 \\ x_{c2} = x_f + (r_0 + r_1)\cos\theta_1 + l_2\cos(\theta_1 + \theta_2) \\ y_{c2} = y_f + (r_0 + r_1)\sin\theta_1 + l_2\sin(\theta_1 + \theta_2) \\ x_{c3} = x_f + r_0\cos\theta_1 + l_3\cos(\theta_1 + \theta_2) \\ y_{c3} = y_f + r_0\sin\theta_1 + l_3\sin(\theta_1 + \theta_2) \\ x_{c4} = x_f + r_0\cos\theta_1 + r_3\cos(\theta_1 + \theta_2) + l_4\cos(\theta_1 + \alpha) \\ y_{c4} = y_f + r_0\sin\theta_1 + r_3\sin(\theta_1 + \theta_2) + l_4\sin(\theta_1 + \alpha) \\ x_{c5} = x_f + r_0\cos\theta_1 + r_3\cos(\theta_1 + \theta_2) + l_5\cos(\theta_1 + \beta) \\ \qquad + r_5\cos(\theta_1 + \beta + \theta_5) \\ y_{c5} = y_f + r_0\sin\theta_1 + r_3\sin(\theta_1 + \theta_2) + l_5\sin(\theta_1 + \beta) \\ \qquad + r_5\sin(\theta_1 + \beta + \theta_5) \end{cases} \tag{2}$$

where $x_f$ and $y_f$ are the coordinates of the robot's foot. The position $(x_c, y_c)$ of the COM of the robot is as follows

$$\begin{cases} x_c = \sum_1^5 m_i x_{ci} / \sum_1^5 m_i \\ y_c = \sum_1^5 m_i y_{ci} / \sum_1^5 m_i \end{cases} \tag{3}$$

In order to simplify the problem we assume the four-bar mechanism is a parallelogram. So we have $r_1 = r_4$, $r_2 = r_3$, $\theta_2 = \theta_3$, and $\theta_3 + \theta_4 = \pi$. The jumping process consists of the stance phase and the flight phase. During the stance phase, the pole leg dose not rotate, the robot has two degrees of freedom

(DOF). We use $\theta_1$ and $\theta_2$ as independent variables to represent the two DOFs. During the flight phase, the robot has five degrees of freedom. $x_f$, $y_f$, $\theta_1$, $\theta_2$, and $\theta_5$ are used to represent the five DOFs.

### B. Dynamic Modeling

The ground reaction forces on the foot are as follows

$$\begin{cases} F_x = \sum_1^5 m_i \ddot{x}_{ci} \\ F_y = \sum_1^5 m_i \ddot{y}_{ci} + \sum_1^5 m_i g \end{cases} \tag{4}$$

In order to simplify the modeling and simulation, we do not consider the joint friction forces of the four-bar mechanism, the damping of the spring, and the air friction force. Assuming the contact point between the lower leg and the ground is an ideal hinge during the stance phase. The robot will take off from the ground when $F_y$ decreases to zero. The dynamic model of jumping is expressed by a Lagrange equation as follows

$$\begin{cases} \frac{d}{dt}\left(\frac{\partial L}{\partial \dot{q}_i}\right) - \left(\frac{\partial L}{\partial q_i}\right) = Q_i \\ L = E_T - V \end{cases} \tag{5}$$

where $E_T$ is the kinetic energy which includes the translational kinetic energy $E_k$ and rotational kinetic energy $E_t$ of the four bars as follows

$$\begin{cases} E_k = \frac{1}{2}\sum_1^5 m_i {v_{ci}}^2 \\ E_t = \frac{1}{2}\sum_1^5 J_i {\omega_i}^2 \end{cases} \tag{6}$$

$V$ is the potential energy which includes the gravitational potential energy $E_g$ of the bars and the elastic potential energy $E_e$ of the torsion spring. $q_i$ are the generalized coordinates and $Q_i$ are the generalized forces.

The free position of the torsion spring is $\pi/2$ when there is no energy stored in the spring. The equilibrium position of the spring is 0 rad when it is fully loaded. As shown in Fig. 1, $\theta_4$ has the relationship with the compression angle $\theta$ of the torsion spring, $\theta_4 = \theta + \pi/6$. Because $\theta_2 = \theta_3$, and $\theta_3 + \theta_4 = \pi$, so $\theta = 5\pi/6 - \theta_2$. $\theta_2$ decreases from $5\pi/6$ to $\pi/3$ when $\theta$ increases from 0 rad to $\pi/2$ during the stretching of the spring. $E_g$ and $E_e$ are as follows

$$\begin{cases} E_g = \sum_1^5 m_i g y_{ci} \\ E_e = \frac{1}{2}K\left(\frac{\pi}{2} - \theta\right)^2 = \frac{1}{2}K\left(\theta_2 - \frac{\pi}{3}\right)^2 \end{cases} \tag{7}$$

where $K$ is the stiffness coefficient of the torsion spring. When the spring is triggered, the stored energy is released and the robot obtains an initial velocity. The robot takes off when the vertical reaction force $F_y$ on the foot of the robot is zero.

In the stance phase, the generalized coordinates $q_i$ are [$\theta_1$, $\theta_2$] and the generalized forces $Q_i$ are [0, 0]. While in the flight phase, $q_i$ are [$x_f$, $y_f$, $\theta_1$, $\theta_2$, $\theta_5$], and $Q_i$ are [0, 0, 0, 0, $M$]. Here, $M$ is the driving torque of the adjusting motor mounted on the joint between the pole leg and the body. From (5), we can derive two and five second-order nonlinear differential equations in the stance and flight phases respectively. These equations will be solved by the ordinary differential equation solver ode45.

## IV. Simulation

In this section, the aerial posture changes and landing postures of the robot are simulated to verify the proposed posture active adjustment method. Firstly, the jumping simulation without pole leg adjustment is conducted. Then, the jumping is simulated when the pole leg rotates around the body driven by the adjusting motor. Lastly, the effects of the length of the pole leg, the mass of the AW, and the driving torque of the adjusting motor on aerial posture adjustment performances are studied.

The parameters of the robot in simulations are $m_1$ = 13 g, $m_2$ = 1.4 g, $m_3$ = 12 g, $m_4$ = 100 g, $r_0$ = 7 cm, $r_1$ = 3.3 cm, $r_2$ = 7.9 cm, $r_3$ = 7.9 cm, $r_4$ = 3.3 cm, $l_1$ = 5.15 cm, $l_2$ = 3.95 cm, $l_3$ = 3.95 cm, $l_4$ = 2 cm, $\alpha$ = 0.868 rad, $\beta$ = 0.349 rad, $J_1$ = 4.60e−5 kg·m$^2$, $J_2$ = 2.98e−6 kg·m$^2$, $J_3$ = 2.50e−5 kg·m$^2$, $J_4$ = 5.67e−5 kg·m$^2$, and $K$ = 2.1585 N·m/rad. Other parameters

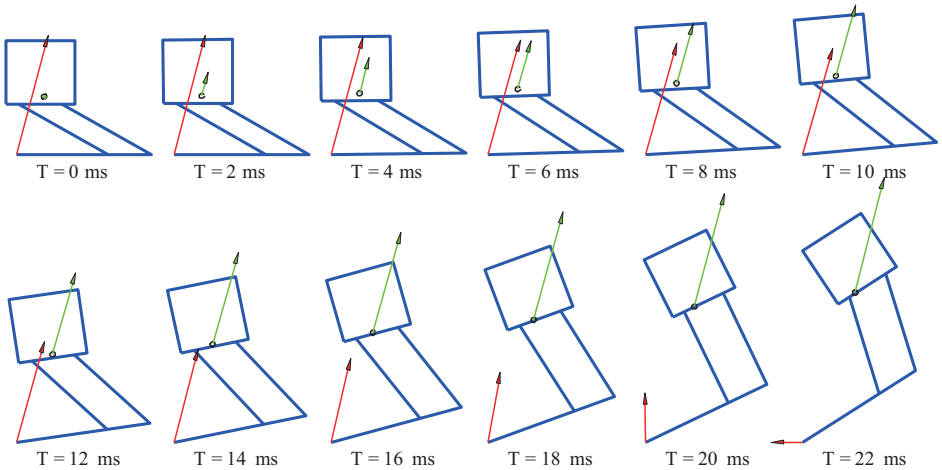


Fig. 2. Stick diagrams of the jumping robot during stance phase without the pole leg mechanism for posture adjusting.

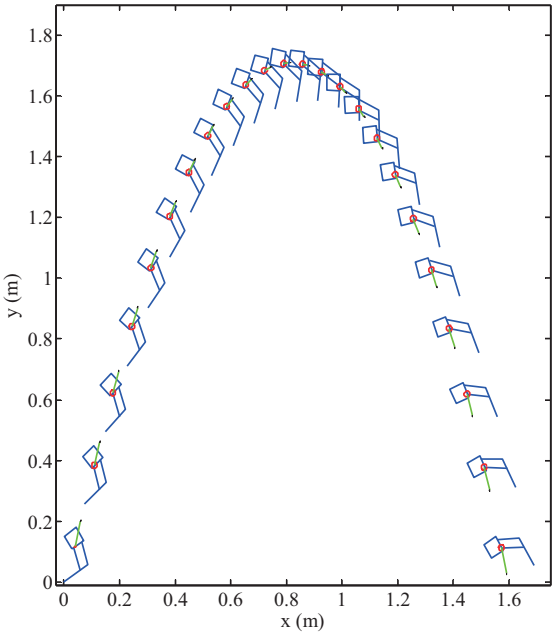


Fig. 3. Stick diagram of the jumping robot during flight phase without the pole leg mechanism for posture adjusting.

including $m_5$, $r_5$, $J_5$, and the driving torque $M$ are decided in different simulations.

### A. Jumping without Aerial Posture Adjustment

The initial conditions of the stance phase are $\theta_1 = 0$ rad, $\theta_2 = 5\pi/6$, and their velocities of 0 rad/s. The stick diagram of the robot during this phase is shown in Fig. 2. The blue lines are the four-bar mechanism. The red lines with arrows represent the ground reaction forces. Their lengths are 0.2% of the sizes of the forces. The black circles depict the COM of the robot. The green lines show the velocities of the robot with lengths of 1.5% of their sizes. From the stick diagram we can see that $\theta_1$ increases slowly while $\theta_2$ decreases gradually when the robot prepares to take off. We can get the ending time $t$ = 0.0223 s when $F_y$ decreases to zero. At the ending time, $\theta_1$ is 0.575 rad, and $\theta_2$ is 1.290 rad, their velocities are 66.755 rad/s and −143.105 rad/s, the horizontal and vertical displacements of the COM are $X_c$ = 0.040 m, and $Y_c$ = 0.117 m, and their velocities are $V_x$ = 1.335 m/s, $V_y$ = 5.451 m/s. The takeoff velocity is $V_c$ = 5.612 m/s and the takeoff angle is 76.239°.

The initial conditions of the flight phase are $x_f$ = 0 m, $y_f$ = 0 m, their velocities of 0 m/s, $\theta_1$ = 0.575 rad, $\theta_2$ = 1.290 rad, their velocities of 66.755 rad/s and −143.105 rad/s. The stick diagram of the robot is illustrated in Fig. 3. The trajectory of the robot's COM is a parabolic curve. The jumping height and distance are about 1.71 m and 1.59 m respectively. The lower leg touches the ground during landing of the robot.

### B. Jumping with Aerial Posture Active Adjustment

The adjusting performance with a pole leg is simulated in this section. The parameters of $m_5$, $r_5$, $J_5$, and the driving torque $M$ are 4 g, 8 cm, 2.56e−5 kg·m$^2$, and −7.0e−4 N·m respectively. The initial conditions of the stance phase are $\theta_1$ = 0 rad, $\theta_2 = 5\pi/6$, and their velocities of 0 rad/s. $\theta_5$ keeps fixed at $\pi/3$. The stick diagram of the robot during this phase is shown in Fig. 4. At the ending time $t$ = 0.0226 s, $\theta_1$ is 0.540 rad, and $\theta_2$ is 1.335 rad, their velocities are 61.389 rad/s and −133.983 rad/s, the horizontal and vertical velocities are $V_x$ = 1.343 m/s, $V_y$ = 5.334 m/s. The takeoff velocity and angle are 5.394 m/s and 75.560° respectively which are smaller than the simulation results without the pole leg mechanism.

The initial conditions of the flight phase are $x_f$ = 0 m, $y_f$ = 0 m, their velocities of 0 m/s, $\theta_1$ = 0.540 rad, $\theta_2$ = 1.335 rad, their velocities of 61.389 rad/s and −133.983 rad/s, $\theta_5$ and its velocity are $\pi/3$ and 0 rad/s. The stick diagram of the robot is shown in Fig. 5. The trajectory of the robot is also a parabolic curve. The pole leg rotates about 61.47 rad relative to the body in the air to adjust its orientation. The rotational angle of

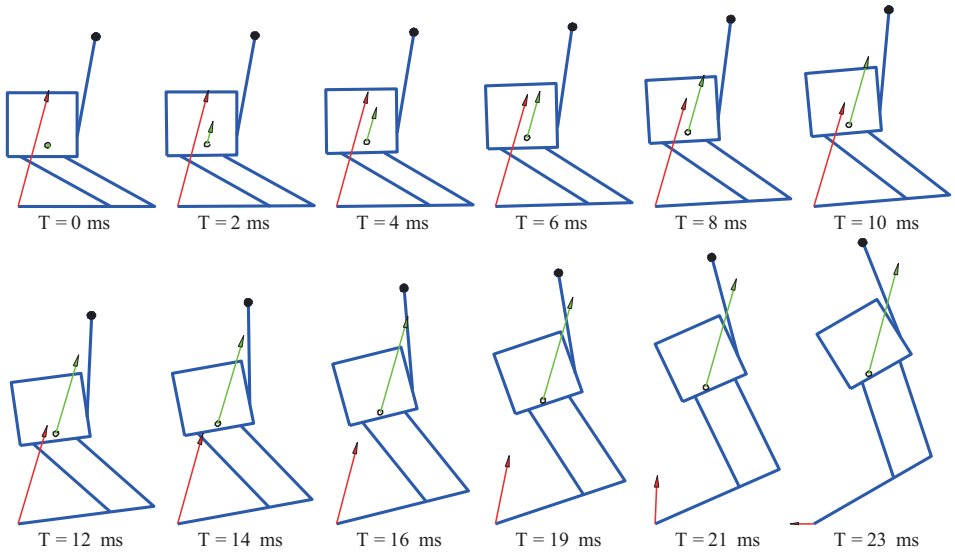


Fig. 4. Stick diagrams of the jumping robot during stance phase with the pole leg mechanism. The angle between the pole leg and the body keeps fixed in this period.

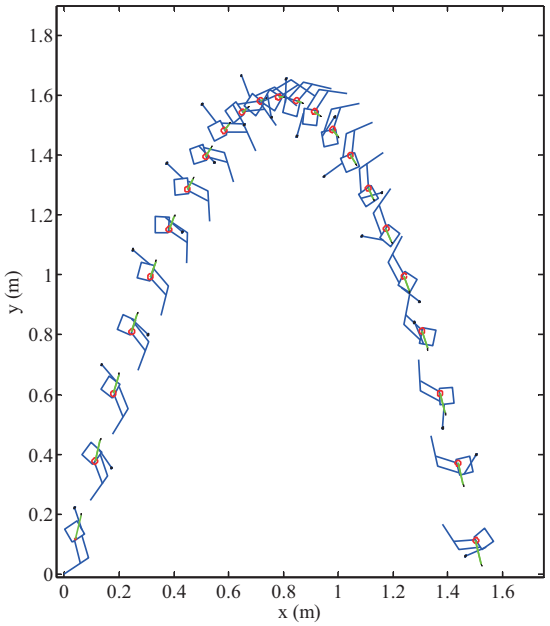


Fig. 5. Stick diagrams of the jumping robot during flight phase with the pole leg mechanism. The angle between the pole leg and the body is adjusted by motor mounted on the joint.

the robot is 5.43 rad. The front surface of the body and the assistant leg touch the ground simultaneously which can protect the lower leg from damage. The pole leg is nearly parallel to the front surface of the body which will avoid the damage of the pole leg. From the simulation results, we can find that the landing posture is safer with aerial posture active adjustment than without it.

### C. Aerial Posture Adjustment at Different Parameters

In this section, the aerial posture adjustment performances at different parameters including length of the pole leg, mass of the AW, and driving torque of the adjusting motor are investigated by simulations.

*1) Effects of Length $r_5$ on Adjustment Performance:* All the initial conditions of the stance phase are the same ones as that in Section IV B except for $r_5$ and $J_5$. Here, $r_5$ increases from 1cm to 10 cm with the step of 0.5 cm while $m_5 = 4$ g and $M =$ −7.0e−4 N·m. The simulation results are shown in Fig. 6. The rotational angle of the robot increases from 2.438 rad to 5.762 rad in the changing range of $r_5$. The angle is 5.45 rad at $r_5 = 8$ cm. This angle is close to 5.43 rad as shown in Fig. 5. The robot will land with a safe posture. The rotational angle of the pole leg drops in the beginning to −259.6 rad and then increases slowly to 62.36 rad. The rotational angle of the pole leg at $r_5 = 8$ cm is 61.97 rad which is also close to 61.46 rad in the simulation results shown in Fig. 5. So, the pole leg does not contact on the ground during landing of the robot.

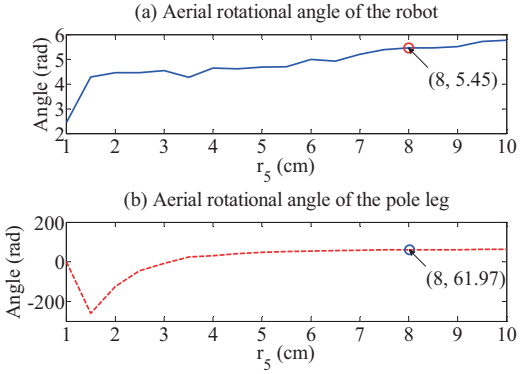


Fig. 6. The length of $r_5$ on aerial posture adjusting performances. (a) and (b) are the rotational angles of the robot and the pole leg.

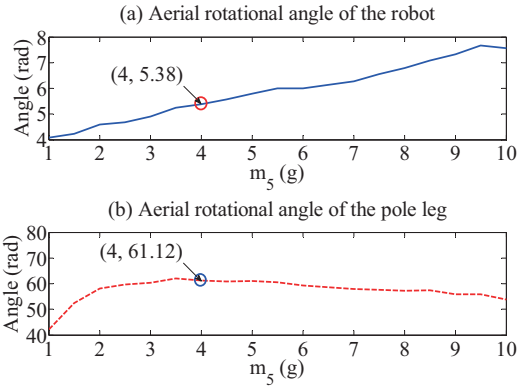


Fig. 7. The mass of $m_5$ on aerial posture adjusting performances. (a) and (b) are the rotational angles of the robot and the pole leg.

*2) Effects of mass $m_5$ on Adjustment Performance:* In these simulations, $m_5$ increases from 1 g to 10 g with the step of 0.5 g while $r_5$ = 8 cm and $M$ = −7.0e−4 N·m. The simulation results are shown in Fig. 7. The rotational angle of the robot is 5.38 rad at $m_5 = 4$ g. This angle is near to the one shown in Fig. 5. The robot lands safely at $m_5 = 4$ g. The rotational angle of the pole leg is 61.12 rad. So, the pole leg will not contact the ground before the body and assistant leg contact the ground.

*3) Effects of Torque M on Adjustment Performance:* The torque $M$ of the adjusting motor can be adjusted by its driving voltage. The torque $M$ of the adjusting motor also has influences on the aerial posture adjusting performances as shown in Fig. 8. The rotational angles of the robot and the pole leg have opposite changing tendency with the increase of

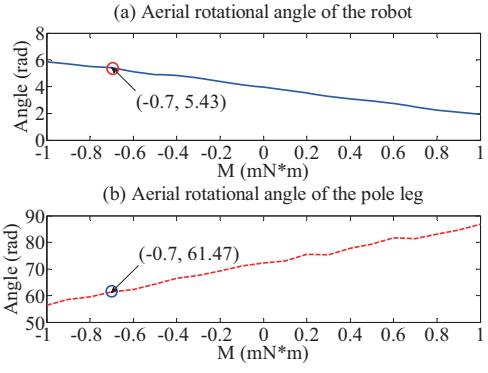


Fig. 8. The driving torque on aerial posture adjusting performances. (a) and (b) are the rotational angles of the robot and the pole leg.

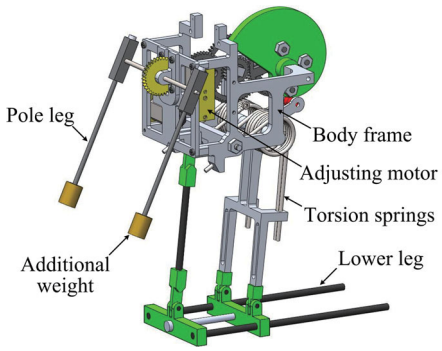


Fig. 9. 3D model of the jumping robot with the new aerial posture adjustment mechanism.

the torque $M$ from −1.0e−3 N·m to 1.0e−3 N·m with the step of 1.0e−4 N·m while $r_5$ = 8 cm and $m_5$ = 4 g. The rotational angles of the robot and the pole leg are 5.43 rad and 61.47 rad at $M$ = −7.0e−4 N·m which are almost the same results as shown in Fig. 5.

## V. Conclusions and Future Work

In this paper, we study the aerial posture adjustment of a jumping robot for its safe landing by modeling and simulation. A pole leg mechanism with an additional weight fixed at its end point like a leg or a tail of animals is mounted on the front surface of the robot. The pole leg can rotate relative to the body of the robot. The simulation results without and with the proposed pole leg mechanism verify the feasibility of the aerial posture adjustment method. The effects of the length of the pole leg, the mass of the AW, and the joint driving torque on aerial posture adjustment performances are also investigated by simulations. The results shown that we can obtain a safe landing posture for protecting the lower leg and the pole leg by selecting proper parameters of the adjusting mechanism.

A 3D model of the jumping robot is designed as shown in Fig. 9. Future work will focus on refining the robot model and fabricating the robot prototype. The aerial posture sensing and controlling of the robot also will be investigated. Experimental tests will be done to provide validations of the aerial posture adjustment method.

## References

[1] N. Carlési and A. Chemori, "Nonlinear Model Predictive Running Control of Kangaroo Robot: a One-Leg Planar Underactuated Hopping Robot," in *Proc. IEEE/RSJ Int. Conf. Intell. Rob. Syst.*, Taipei, Taiwan, Oct. 18-22, 2010, pp. 3634–3639.

[2] Q. V. Nguyen and H. C. Park, "Design and demonstration of a locust-like jumping mechanism for small-scale robots," *J. Bionic Eng.*, vol. 9, no. 3, pp. 271–281, 2012.

[3] F. Li, W. Liu, X. Fu, G. Bonsignori, U. Scarfogliero, et al., "Jumping like an insect: design and dynamic optimization of a jumping mini robot based on bio-mimetic inspiration," *Mechatronics*, vol. 22, no. 2, pp. 167–176, 2012.

[4] K. Je-Sung, J. Sun-Pill, N. Minkyun, K. Seung-Won, and C. Kyu-Jin, "Flea inspired catapult mechanism with active energy storage and release for small scale jumping robot," in *Proc. IEEE Int. Conf. Rob. Auto.*, Karlsruhe, Germany, May 6-10, 2013, pp. 26–31.

[5] S.D. Howe, R.C. Obrien, R.M. Ambrosi, B. Gross, J. Katalenich, et al., "The mars hopper: an impulse driven, long range, long-lived mobile platform utilizing in-situ Martian resources," *Acta Astronaut*, vol. 69, no. 11-12, pp. 1050–1056, 2011.

[6] E. Ackerman, "Boston dynamics sand flea robot demonstrates astonishing jumping skills," *IEEE Spectrum Robot.* Blog, Mar. 22, 2012.

[7] D. Chen, J. Yin, Y. Huang, K. Zhao, T. Wang, "A hopping-righting mechanism analysis and design of the mobile robot," *J Braz. Soc. Mech. Sci. Eng.*, vol. 35, no. 4, pp. 469–478, 2013.

[8] M. Kovač, M. Schlegel, J. Zufferey, and D. Floreano, "Steerable miniature jumping robot," *Auton. Robots*, vol. 28, no. 3, pp. 295–306, 2010.

[9] J. Zhao, J. Xu, B. Gao, N. Xi, F.J. Cintrón, M.W. Mutka, L. Xiao, "MSU Jumper: A Single-Motor-Actuated Miniature Steerable Jumping Robot," *IEEE Trans. Rob.*, vol. 29, no. 3, pp. 602–614, 2013.

[10] S. A. Stoeter and N. Papanikolopoulos, "Kinematic motion model for jumping scout robots," *IEEE Trans. Robot. Autom.*, vol. 22, no. 2, pp. 398–403, Apr. 2006.

[11] J. A. Smith, I. Sharf, and M. Trentini, "Bounding gait in a hybrid wheeled-Leg robot," in *Proc. IEEE/RJS Int. Conf. Intell. Rob. Syst.*, Beijing, China, Oct. 9–15, 2006. pp. 5750–5755.

[12] J. A. Smith, I. Poulakakis, M. Trentini, I. Sharf, "Bounding with active wheels and liftoff angle velocity adjustment," *International Journal of Robotics Research*, vol. 29, no. 4, pp. 414–427, 2010.

[13] R. Armour, K. Paskins, A. Bowyer, J. F. V. Vincent, and W. Megill, "Jumping robots: a biomimetic solution to locomotion across rough terrain," *Bioinspiratoin and Biomimetics*, vol. 2, pp. 65–82, Jun. 2007.

[14] T. Ho, and S. Lee, "A novel design of a robot that can jump and roll with a single actuator," in: *Proc. IEEE/RJS Int. Conf. Intell. Rob. Syst.*, Vilamoura, Algarve, Portugal, Oct. 7–12, 2012, pp. 908–913.

[15] D. H. Kim, J. H. Lee, I. Kim, S. H. Noh, and S. K. Oho, "Mechanism, control, and visual management of a jumping robot," *Mechatronics*, vol. 18, no. 10, pp. 591–600, 2008.

[16] G. Song, K. Yin, Y. Zhou, and X. Cheng, "A surveillance robot with hopping capabilities for home security," *IEEE Trans. on Consum. Electron.* 2009, vol. 55, no. 4, pp. 2034–2039.

[17] D. C. Dunbar, "Aerial maneuvers of leaping lemurs: the physics of whole-body rotations while airborne," *Am. J. Primatol.*, vol. 16, pp. 291–303, 1988.

[18] C. Walker, C. J. Vierck Jr., and L. A. Ritz, "Balance in the cat: role of the tail and effects of sacrocaudal transaction," *Behavioural Brain Research*, vol. 91, pp. 41–47, 1998.

[19] A. Jusufi, D. I. Goldman, S. Revzen, and R. J. Full, "Active tails enhance arboreal acrobatics in geckos," in *Proc. of the National Academy of Sciences of the United States of America*, vol. 105, no. 11, pp. 4215–4219, Mar. 18, 2008.

[20] T. Libby, T. Moore, E. Chang-Siu, D. Li, D. Cohen, A. Jusufi, and R. Full, "Tail-assisted pitch control in lizards, robots and dinosaurs," *Nature*, vol. 481, pp. 181–184, 2012.

[21] Gal Ribak, Moshe Gish, Daniel Weihs, and Moshe Inbar, "Adaptive aerial righting during the escape dropping of wingless pea aphids," *Current Biology*, vol. 23, no 3, pp. R102–R103, Feb. 2013.

[22] L. Han, Z. Wang, A. Ji, and Z. Dai, "The Mechanics and Trajectory Control in Locust Jumping," *Journal of Bionic Engineering*, vol. 10, no. 2, pp 194–200, 2013.

[23] E. Chang-Siu, T. Libby, M. Tomizuka and R. J. Full, "A lizard-inspired active tail enables rapid maneuvers and dynamic stabilization in a terrestrial robot," in *Proc. IEEE/RJS Int. Conf. Intell. Rob. Syst.*, San Fransisco, CA, USA, Sep. 25–30, 2011, pp. 1887–1894.

[24] A. M. Johnson, T. Libby, E. Chang-Siu, M. Tomizuka, R. J. Full, and D. E. Koditschek, "Tail assisted dynamic self righting," in *Proc. Int. Conf. Climbing Walking Rob. Support Technol. Mob. Mach., CLAWAR*, Baltimore, MD, United states, Jul. 23–26, 2012, pp. 611–620.

[25] J. Zhao, T. Zhao, N. Xi, F. J. Cintrón, Matt W. Mutka, and Li Xiao, "Controlling aerial maneuvering of a miniature jumping robot using its tail," in *Proc. IEEE/RJS Int. Conf. Intell. Rob. Syst.*, Tokyo, Japan, Nov. 3–7, 2013, pp. 3802–3807.

[26] J. Zhang, G. Song, Y. Li, G. Qiao, A. Song, and A. Wang, "A Bio-Inspired Jumping Robot: Modeling, Simulation, Design, and Experimental Results," *Mechatronics*, vol. 23, no. 8, pp. 1123–1140, Dec. 2013.